Magnetotunneling spectroscopy of one-dimensional wires

B. Kardynał, C. H. W. Barnes, E. H. Linfield, D. A. Ritchie, J. T. Nicholls, K. M. Brown, G. A. C. Jones, and M. Pepper
Cavendish Laboratory, Madingley Road, Cambridge, CB3 0HE, United Kingdom
(Received 4 November 1996)

We present results of a detailed study of equilibrium magnetotunneling between an array of independent identical one-dimensional wires and a two-dimensional electron gas. From the tunneling differential conductance, measured as a function of the in-plane magnetic field, we find directly the number of occupied one-dimensional subbands, the subband energies, and the wave functions as a function of the strength of confinement in these wires. As many as 14 one-dimensional subbands were probed. We show that an analysis of our results based on the Bardeen tunneling Hamiltonian formalism allows the determination of the functional form of one-dimensional confining potentials. We give two examples, one for a narrow wire and one for a wide wire. [S0163-1829(97)51804-2]

The Schottky gate technique for patterning two-dimensional electron gases (2DEG's) (Ref. 1) in GaAs/$Al_xGa_{1-x}As$ heterostructures initiated an intensive study of one-dimensional (1D) systems.[2] The response of these systems to changing gate voltage is a complex problem—experimentally and theoretically. Theoretical models,[3] which predict a generic dependence of the 1D confining potential on gate voltage, at least must make assumptions about the distribution of ionized donors, strain introduced by the surface gates and the nature of surface states and include a model for the Schottky interface. The uncertainty in these parameters has provided a strong motivation for experimental investigation of quantum-mechanical structure in these systems. Equilibrium lateral transport[4] and capacitance measurements[5,6] may not be used for this purpose since they yield information only about density of states at the chemical potential. Nonequilibrium conductance measurements allow the determination of subband spacings close to the chemical potential,[7] and magnetodepopulation of 1D channels can be used to estimate the width of confining potentials with many occupied subbands.[8] However, these methods do not provide sufficient information to determine accurate functional forms for confining potentials. Tunneling experiments, in which electrons from a detector electron gas, are used to probe a 1D system do in principle provide sufficient information to determine all quantum-mechanical structures. This is because conservation of momentum in tunneling ensures that these measurements are sensitive to the details of the 1D spectral function.[9] This function contains the Fourier transforms of the occupied eigenstates,[10,11] and allowed approximate forms for bound states in etched 1D wires[12] to be determined in nonequilibrium measurements.

In this paper we present the results of equilibrium magnetotunneling experiments on electrostatically defined 1D wires which allow a direct determination of their eigenvalues and wave functions, and therefore the functional forms of their confining potentials.

Figure 1 shows a schematic diagram of our device.[13] Two parallel 2DEG's occupy 18-nm-wide GaAs quantum wells, which are separated by a 12.5-nm-wide $Al_{0.33}Ga_{0.67}As$ barrier. The carrier concentrations are 3.0×10^{15} and 1.9×10^{15} m^{-2}, with corresponding low-temperature mobilities of 50 and 20 $m^2\ (V\ s)^{-1}$ in the upper and lower wells, respectively. Separate contact to each 2DEG was achieved using a selective depletion scheme.[14] An *in situ* patterned n^+ GaAs full gate[15] beneath the active tunneling area was used to fix the carrier concentration in the lower 2DEG at 3.0×10^{15} m^{-2} by applying a voltage $V_{bg}=+0.6$ V. A superlattice Schottky gate was defined above the active tunneling area using electron-beam lithography. Here we consider two devices with superlattice periods of 350 and 570 nm, and lithographic wire widths of 180 and 340 nm, respectively, each consisting of 50 wires. The application of a voltage $V_{sl}^{def}=-0.42$ V was necessary to define an array of independent quasi-1D wires in the upper well of each device. Due to the penetration of the superlattice gate electric field through the depleted regions of the upper well, a 1D surface superlattice (1DSSL) was induced in the lower 2DEG. This device structure has a number of features which make it particularly suitable for determining confining potentials: the experiments may be performed in equilibrium, thereby eliminating the effect of capacitive coupling on the confining potential; the widths of the two quantum wells are identical to within atomic resolution, thereby eliminating the effects of relative diamagnetic shift; and the carrier concentration in the detector layer can be tuned to probe the Fermi surface of the 1D wires.

Typical tunneling differential conductance (TDC) characteristics, as measured between the quasi-1D wires and the 1DSSL are shown in Fig. 2 as a function of the magnetic field applied in the plane of the wells, parallel $B_\parallel$, and perpendicular $B_\perp$ to the wires. The measurements were performed at 60 mK, with an excitation voltage of 50 μV at 79 Hz. Figures 2(a) and 2(b) show the results obtained in the

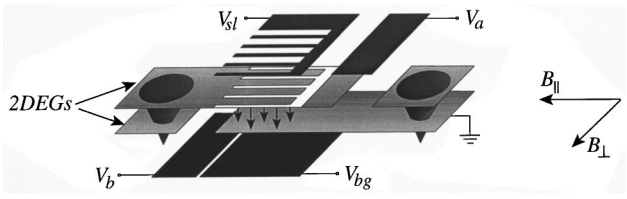

FIG. 1. Schematic diagram of our device geometry. Voltages V_a and V_b make independent contact to each well.

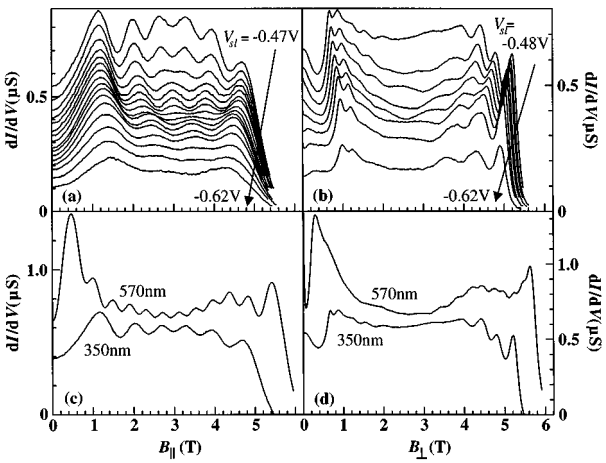

FIG. 2. Magnetotunneling differential conductance measured with the magnetic field applied (a) and (c) parallel and (b) and (d) perpendicular to the wires. Upper graphs compare the TDC for the same, 350-nm period device but different V_{sl} [(a)−0.47,−0.48,. . . , −0.62 V, (b)−0.48,−0.50,. . . ,−0.62 V]. Lower graphs compare the TDC measured for V_{sl}=−0.48V for 350- and 570-nm period devices.

350-nm period device for V_{sl} between −0.48 and −0.62 V. At V_{sl}=− 0.62 V, the lower 2DEG was sufficiently depleted under the 1DSSL gate pattern to prevent further measurements. Figures 2(c) and 2(d) compare results for the 350- and 570-nm period devices at V_{sl}=−0.48 V.

Qualitatively, just as for 2D-2D magnetotunneling,[16] the oscillations in the data can be explained as resulting from the relative displacement of the origins in k space of each quantum well by $\delta k_{(\perp,\parallel)}=ez_0B_{(\parallel,\perp)}/\hbar$, where z_0=30.5 nm is the average tunneling distance between wells. It causes different pairs of k states in each well to contribute to the tunneling at different magnetic fields resulting in a variation in the TDC. The observed change in the TDC upon rotation of the direction of the magnetic field with respect to the 1DSSL therefore reflects directly the asymmetry of the 1D wires.

A quantitative analysis can be obtained using the Bardeen tunneling Hamiltonian formalism.[17] Tunneling between an array of 1D wires and a 1DSSL yields a complex tunneling problem. However, in the upper well of our device the large barriers which separate 1D wires make them independent systems which contribute independently to the device TDC. In the lower well the confining potential is flat and 2DEG-like in the regions where there is a significant overlap between the wave functions in the upper and lower wells[18] due to screening by the 1D wire densities. The low-temperature TDC of our device is therefore a sum of 1D-2D tunneling events, one for each wire, and may be written as an overlap integral between the spectral function of an average 1D system with that of a 2D system:

$$\frac{dI}{dV}\propto t^2\sum_{k_\parallel,k_\perp}A_2(k_\parallel+\delta k_\parallel,k_\perp+\delta k_\perp;\mu)B_1(k_\parallel,k_\perp;\mu), \tag{1}$$

where t^2 is the z-direction transmission coefficient (assumed the energy and position independent), and μ is the chemical potential. The spectral function of the 1D system is defined by

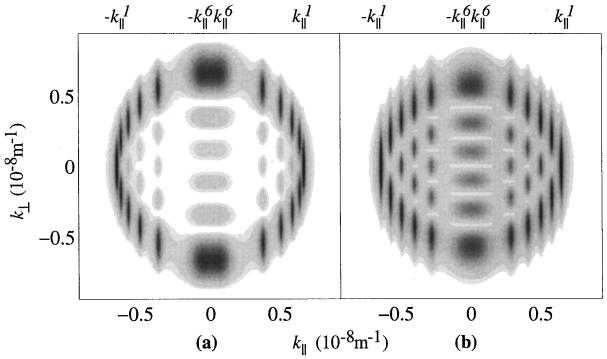

FIG. 3. Spectral functions of a 1D parabolic potential (a) and a 1D square well potential (b), at the chemical potential, for $\Gamma=0.5$ meV.

$$B_1(k_\parallel,k_\perp;\mu)=\sum_\nu|\tilde{\phi}_\nu(k_\perp)|^2A_1(k_\parallel,\nu;\mu), \tag{2}$$

where $\tilde{\phi}_\nu(k_\perp)$ is the Fourier transform of the νth 1D subband wave function. In the quasi-particle approximation the spectral functions of the 1D wire and 2DEG in the basis of their own eigenstates, $A_{(1,2)}$, are Lorentzian

$$A_{(1,2)}(s_{(1,2)};\mu)=\Gamma/2\pi[(\Gamma/2)^2+(\mu-\xi^{(1,2)2}_{s_{(1,2)}})]. \tag{3}$$

$s_1=(k_\parallel,\nu)$, $s_2=(k_\parallel,k_\perp)$ are the quantum numbers of the 1D wire and 2DEG, respectively, and $\hbar/\Gamma$ is the quasiparticle lifetime, but here it will also account for differences between 1D wires. $\Gamma=0.5$ meV was used in the calculations as fitting best the data (compare Ref. 9). $\xi^{(1)}_{s_1}=E_\nu+\hbar^2k_\parallel^2/2m^*+V_1$ is the dispersion relation in the 1D wire and $\xi^{(2)}_{s_2}=\hbar^2(k_\parallel^2+k_\perp^2)/2m^*+V_2$ is the dispersion relation for the 2DEG. E_ν are the 1D subband energies in the upper well and $V_{(1,2)}$ are 2D subband energies in the upper and lower wells, respectively.

The spectral function of a 2DEG, evaluated at the chemical potential, is just the 2DEG's Fermi circle. The spectral function of a 1D wire, evaluated at the chemical potential, is elliptical in k space, and contains an internal structure. Two examples of 1D spectral functions are shown in Figs. 3(a) and 3(b) for a parabolic and square-well potential, respectively. Both have six occupied subbands. The details of the 1D spectral function are separable into $k_\parallel$ and $k_\perp$ dependencies, as may be seen from Eq. (2). In the $k_\parallel$ direction the spectral function has peaks at values of $k_\parallel=k_\parallel^\nu$ derived from $\mu=\xi^{(1)}_{s_1}$, and indicated in Figs. 3(a) and 3(b). In the $k_\perp$ direction, each peak deriving from each subband is modulated by the Fourier spectrum of this subband wave function.

When $B_\parallel$ is swept, the Fermi circle of the 2DEG moves relative to the 1D spectral function in the $k_\perp$ direction. As it passes across the 1D spectral function, there will be a contribution to the TDC from all parts of the 1D spectral function with which it intersects. Detailed analysis of Eq. (1) shows that in general the dominant contribution is from the Fourier spectrum of the highest occupied subband. Since the Fermi circle in the 2DEG was larger than the 1D spectral

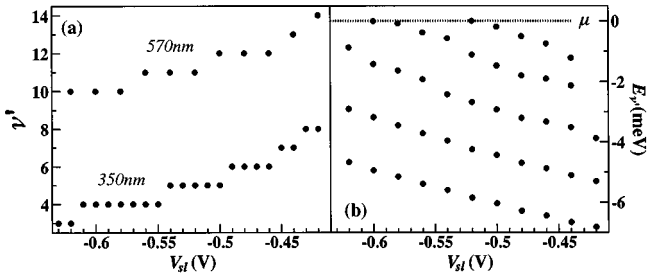

FIG. 4. (a) Depopulation characteristics obtained from TDC sweeps with $B_\parallel$ for 350- and 570-nm period devices. (b) Subband energies estimated from TDC sweeps with $B_\perp$ for the 350-nm period device.

function during the experiments the plots in Figs. 2(a) and 2(c) are full representations of 1D wave functions (or their amplitude) in k space. As we sweep $V_{\rm sl}$ [Fig. 2(a)] or change the lithographic wire width [Fig. 2(c)], the number of peaks in each trace, which is the same as the number of occupied subbands, decreases as the confinement increases. In addition, Fig. 2(a) shows the change in symmetry of the wave functions between odd and even as successive subbands are depopulated. Figure 4(a) shows the number of occupied subbands as a function of $V_{\rm sl}$ taken from such traces for both devices, which follow the well-known 1D subband depopulation characteristics.[4,6] The lowest number of probed subbands was limited by the geometry of the superlattice gate. As many as 14 1D subbands could be probed in the wider device. Up to now the observation of so many subbands has been reported only from measurements of ballistic channels, which have smooth potential profiles.[2] Our result shows that the superlattice gate also produces a smooth potential in the upper well, and may suggest that more complex mechanisms lead to collective depopulation of the subbands.[19]

When $B_\perp$ is swept, the positions of maximum intersection between the 1D and 2DEG spectral functions correspond, approximately, to the fields where the trailing edge of the 2DEG Fermi circle intersects with the quantized values $k_\parallel^\nu$ of the 1D spectral function. From the magnetic-field points at which maximum intersection occurs in experimental traces, we can calculate $k_\parallel^\nu$ and therefore estimate E_ν. These are shown in Fig. 4(b) for the narrower device, for which the peaks are well resolved. They show the expected increase in E_ν with increasing confinement, in agreement with calculations in Ref. 3, but we have insufficient data to show clearly the pinning of the peaks in the 1D density of states at the chemical potential. The subband separation is similar to that found in nonequilibrium lateral measurements.[7]

The spectral functions in Figs. 3(a) and 3(b) are quite different. For the square-well potential the $k_\parallel^\nu$ points are bunched toward large values of $|k_\parallel|$, but for the parabolic potential they are more evenly spaced as a result of their different eigenspectra. In the $k_\perp$ direction for the square-well potential the wave functions are truncated sin and cos functions which have Fourier spectra which peak around the quantized 1D $k_\perp$ values. This gives Fig. 3(a) the appearance of a broad elliptical ring. In the $k_\perp$ direction for the parabolic potential, the simple harmonic-oscillator wave functions are always localized around the classical turning points. This

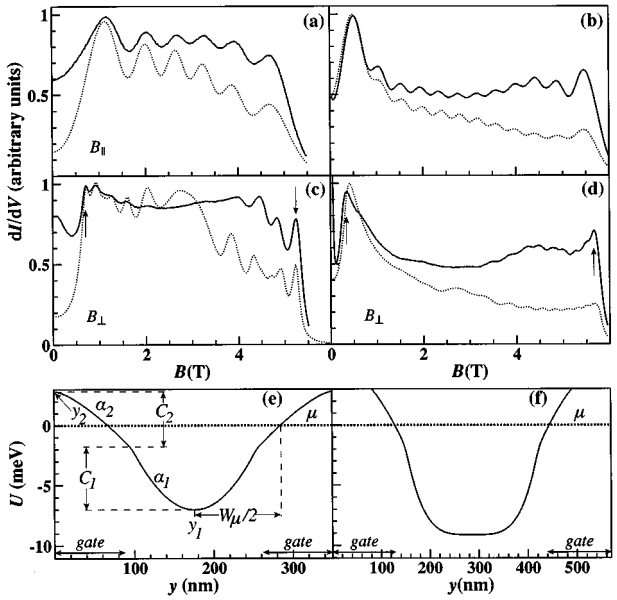

FIG. 5. Experimental and calculated TDC for $V_{\rm sl}=-0.48$ V for $B_\parallel$ (a) and (b) and $B_\perp$ (c) and (d) for a 350-nm period device (a) and (c) and a 570-nm device (b) and (d). (e) shows the best fitting potential profile for 350-nm period device, and (f) for a 570-nm period device.

gives Fig. 3(b) the appearance of a flat elliptical disc. The width of the spectral function in the $k_\perp$ direction is proportional to the reciprocal of the width of the 1D wire at the chemical potential, and the width in the $k_\parallel$ direction is given by E_1.

The differences between spectral functions for different potentials result in very different TDC characteristics.[20] Each measurement of the TDC as a function of in-plane magnetic field is a unique signature of the underlying confining potential, and in principle may be used to extract its functional form. Since the TDC traces for the $B_\parallel$ and $B_\perp$ directions emphasize different aspects of the 1D spectral function, in practice we found it better to use data from both directions to determine confining potential profiles. Figure 5 shows experimental TDC's for $B_\parallel$ and $B_\perp$ sweeps with $V_{\rm sl}=-0.48$ V (solid lines) compared to the TDC calculated from Eq. (1) using functional forms for the confining potentials which gave the closest match between experiment and theory. These potentials are shown in Figs. 5(e) and 5(f). For a narrow wire we find an essentially parabolic confinement, and for the wide wire we find a flat bottomed potential with steep walls. The parameters which define them are shown in Fig. 5(e), and were obtained in the following way. The period of the superlattice $W_{\rm sl}$ is known accurately from calibrated scanning electron microscopy photographs of the device. The data in Figs. 5(a) and 5(b) give us the number of occupied subbands and the spatial extent of the highest occupied subband wave function and therefore the width W_μ. The Fermi energies in each 2DEG and the lowest subband energy E_1 are both determined by the positions of the outermost peaks marked by arrows in Figs. 5(c) and 5(d). These values are very accurate, since these positions are not affected by the internal structure of the 1D spectral function. Approximate eigenvalues can also be found from Figs. 5(c) and 5(d)

and their distribution gives a strong indication of the shape of the confining potential. The lower part of the confining potential defined about point y_1 is taken to be $U \propto |y-y_1|^{\alpha_1}$. This parametrization allows us to vary its shape continuously from triangular $\alpha_1=1$ to square $\alpha_1 \to \infty$. We choose a value for α_1 based on the distribution of peaks in Figs. 5(c) and 5(d), at high and low $B_\parallel$, and the overall shape of the TDC which varies from strongly peaked for a square potential to flat for a parabolic potential (cf. Fig. 3). The shape of the upper part of the confining potential defined around point y_2 is then adjusted through α_2 and C_2 (defined as for the lower part) to give the correct number of occupied subbands and width. Fine overall adjustments are then made to α_1, α_2, C_1, and C_2 to give the best overall fit. It should be noted that the spectral function does not contain any information about unoccupied subbands and therefore the TDC is not sensitive to the shape of the confining potential above the chemical potential. The deviation between the experimental and theoretical TDC derives from tunneling which does not come from the overlap between the 2DEG Fermi circle and the 1D spectral function. It is mostly a slowly varying background which probably comes from the assumption of a uniform 2DEG in the lower well, and the assumption that disorder in the 1D wires is accounted for by a spectral broadening parameter.

In conclusion, we have presented magnetotunneling studies of 1D wires defined by surface Schottky gates, which are able to measure directly eigenenergies and wave functions, and we showed that analysis with the Bardeen tunneling Hamiltonian formalism may be used to determine functional forms of 1D confining potentials. We find that the generic behavior of Laux *et al.*[3] describes our data very well: the subband spacings increase with increasingly negative gate voltage; a narrow wire has a nearly parabolic confining potential, whereas a wide wire has a flat bottom and steep walls. We cannot directly compare our results with Ref. 3, since they perform their calculations for a different device structure. For future work, results from our device should allow an accurate parametrization of this type of calculation. In addition, since equilibrium magnetotunneling depends upon the shape of the spectral function, this device structure can be used to investigate non-Fermi-liquid behavior predicted for 1D systems.[21] Our experiment is an example of what can be done with equilibrium magnetotunneling. The device structure is such that it is possible to perform both magnetotunneling and lateral transport measurements on gate geometries of arbitrary shape.

ACKNOWLEDGMENTS

We thank D. H. Cobden, C. J. B. Ford, and D. Khmelnitskii for useful discussions. B.K. acknowledges support from Trinity College, C.H.W.B. from the I. Newton Trust, and D.A.R. from Toshiba Cambridge Research Centre. This work was funded by the Engineering and Physical Sciences Research Council.

[1] T. Thornton *et al.*, Phys. Rev. Lett. **56**, 1198 (1986).
[2] C. W. J. Beenakker and H. van Houten, in *Solid State Physics*, edited by H. Ehrenreich and D. Turnbull (Academic, San Diego, 1991), Vol. 44.
[3] S. E. Laux *et al.*, Surf. Sci. **196**, 101 (1986).
[4] D. A. Wharam *et al.*, J. Phys. C **21**, L209 (1988); B. J. van Wees *et al.*, Phys. Rev. Lett. **60**, 848 (1988).
[5] T. P. Smith III *et al.*, Phys. Rev. Lett. **61**, 585 (1988).
[6] H. Drexler *et al.*, Phys. Rev. B **49**, 14 074 (1994).
[7] N. K. Patel *et al.*, Phys. Rev. B **44** 13 549 (1991).
[8] K.-F. Berggren *et al.*, Phys. Rev. Lett. **57**, 1769 (1986).
[9] B. Kardynał *et al.*, Phys. Rev. Lett. **76**, 3802 (1996).
[10] W. Demmerle *et al.*, Phys. Rev. B **47**, 13 574 (1993).
[11] N. Mori *et al.*, Phys. Rev. B **51**, 1735 (1995).
[12] P. H. Beton *et al.*, Phys. Rev. Lett. **75**, 1996 (1995).
[13] B. Kardynał *et al.*, Appl. Phys. Lett. **68**, 826 (1996).
[14] J. P. Eisenstein *et al.*, Appl. Phys. Lett. **58**, 1497 (1991); K. M. Brown *et al.*, J. Vac. Sci. Technol. B **12**, 1293 (1994).
[15] E. H. Linfield *et al.*, Semicond. Sci. Technol. **8**, 415 (1993).
[16] J. P. Eisenstein *et al.*, Phys. Rev. B **44**, 6511 (1991).
[17] J. Bardeen, Phys. Rev. Lett. **6**, 57 (1961).
[18] F. Stern (private communication).
[19] Y Sun and G. Kirczenow, Phys. Rev. Lett. **72**, 2450 (1994).
[20] B. Kardynał, Ph.D thesis, Cambridge, U.K., 1995.
[21] L. I. Glazman *et al.*, Phys. Rev. B **45**, 8454 (1992); F. D. M. Haldane, J. Phys. C **14**, 2585 (1981).